BNL-225842-2024-TECH
EIC-ADD-TN-100

Formalism for Local Correction of Vertical Crabbing in Hadron Storage Ring

D. Xu

July 2024

Electron-Ion Collider Project

Brookhaven National Laboratory

U.S. Department of Energy

USDOE Office of Science (SC), Nuclear Physics (NP)

Notice: This technical note has been authored by employees of Brookhaven Science Associates, LLC under Contract No.DE-SC0012704 with the U.S. Department of Energy. The publisher by accepting the technical note for publication acknowledges that the United States Government retains a non-exclusive, paid-up, irrevocable, world-wide license to publish or reproduce the published form of this technical note, or allow others to do so, for United States Government purposes.

DISCLAIMER

This report was prepared as an account of work sponsored by an agency of the United States Government. Neither the United States Government nor any agency thereof, nor any of their employees, nor any of their contractors, subcontractors, or their employees, makes any warranty, express or implied, or assumes any legal liability or responsibility for the accuracy, completeness, or any third party's use or the results of such use of any information, apparatus, product, or process disclosed, or represents that its use would not infringe privately owned rights. Reference herein to any specific commercial product, process, or service by trade name, trademark, manufacturer, or otherwise, does not necessarily constitute or imply its endorsement, recommendation, or favoring by the United States Government or any agency thereof or its contractors or subcontractors. The views and opinions of authors expressed herein do not necessarily state or reflect those of the United States Government or any agency thereof.

Formalism for Local Correction of Vertical Crabbing in Hadron Storage Ring

Derong Xu*
Brookhaven National Laboratory
(Dated: July 26, 2024)

The Electron-Ion Collider (EIC) incorporates crab cavities in both the Electron Storage Ring (ESR) and the Hadron Storage Ring (HSR) to achieve unprecedented luminosity goals. This technical note presents a formalism for the local correction of vertical crabbing in the HSR, addressing the complexities introduced by the integration of crab cavities and the interplay between betatron coupling and crabbing dispersion. Various strategies, including the use of skew quadrupoles and adjustments of Twiss functions, are explored to compensate vertical crabbing to achieve optimal beam-beam performance. The derived theoretical formulas offer practical guidance for minimizing the required vertical crabbing corrections, and will be implemented in the HSR lattice design.

I. INTRODUCTION

The Electron-Ion Collider (EIC) incorporates crab cavities in both the Electron Storage Ring (ESR) and the Hadron Storage Ring (HSR) to achieve its unprecedented luminosity goals [1]. In principle, the downstream crab cavities are designed to compensate for the crabbing effect introduced by the upstream crab cavities, ensuring that the crabbing tilt is confined within the Interaction Region (IR). This approach has been successfully implemented in the ESR by strategically relocating one side crab cavities [2]. However, in the HSR, the crabbing is not fully closed.

The IR of the HSR is a complex and densely packed area, necessitating careful planning and precise engineering to accommodate the array of essential components [3]. Among these, the crab cavities, occupying a length of 15 meters, require a horizontal beta function (β_x) of 1300 meters to provide crab kick for beams up to 275 GeV. Additionally, the incorporation of spin rotators and the Siberian snake, essential for rotating and preserving the spin orientation, along with the detector instrumentation, demand enough installation space. The dipoles at the IR are arranged to serve multiple purposes: establishing the required crossing angle, separating collision products from the stored beam, and preventing geometrical conflicts between different machines. In navigating these requirements, the horizontal phase advance from the upstream to the downstream crab cavity has been finely tuned to 175°. Nevertheless, this setup falls 5° short of the ideal, resulting in crabbing leaking out of the IR. Given the intricate geometry and significant beta function demands, relocating the crab cavity, as done in the ESR, is not feasible. Consequently, the HSR must contend with the unavoidable leakage of crabbing.

The beam tilting can be described by the concept of crab dispersion, as detailed in reference [4]. Similar to the definition of momentum dispersion, the crab dispersion can be defined as:

$$\boldsymbol{\zeta}^* = \left(\frac{\partial x}{\partial z}, \frac{\partial p_x}{\partial z}, \frac{\partial y}{\partial z}, \frac{\partial p_y}{\partial z}, \right)^{\mathrm{T}} \tag{1}$$

To optimize beam-beam performance, it is essential to match the crab and momentum dispersion at the interaction point (IP) defined by:

$$\boldsymbol{\zeta}^* = (-\theta_c, 0, 0, 0)^{\mathrm{T}}, \qquad \boldsymbol{\eta}^* = (0, 0, 0, 0)^{\mathrm{T}} \tag{2}$$

where ζ, η denotes crab, momentum dispersion respectively. Weak-strong beam-beam simulations indicate large tolerance in ζ_2^* and η_2^*. Nonetheless, the detector's requirements for nearly equal horizontal and vertical divergences necessitate precise adherence to these matching conditions. There are also some tolerances on other three dimensions, $\zeta_{1,2,4}$ and $\eta_{1,2,4}$. However, it is necessary to correct them to ideal values in the simulation to verify the capability of our correction system. Therefore, Eq. (2) should be exactly matched in the design process.

When the vertical crabbing is included, a general procedure to correct dispersion and betatron coupling can be:

(1) **Disable RF and Crab Cavities:** Begin by turning off the RF and crab cavities. Initiate betatron decoupling through the adjustment of skew quadrupoles to eliminate coupling effects.

* dxu@bnl.gov

(2) **Crabbing adjustment:** Calculate the necessary horizontal and vertical crabbing based on linear model to determine the optimal settings.

(3) **Activate RF and Crab Cavities:** Reactivate the RF and crab cavities. The momentum dispersion at these cavities, along with a non-zero longitudinal tune, will disrupt the previously established conditions of Eq.(2). Consequently, make minor adjustments to all available control knobs to re-align the system with Eq. (2).

(4) **Fine-Tuning Outside IR:** Adjust the control knobs located outside the Interaction Region (IR) to fine-tune the working point, restoring the linear beam dynamics to the design value.

Among them, step (1) addresses the betatron coupling, while step (2) is focused on correcting dispersion. In step (3), the combined effects of crab and momentum dispersion are considered; these effects are small in the HSR due to the significant separation between the longitudinal and transverse tunes. Step (4) involves adjustments using knobs located outside the IR, which do not interfere with the processes of the preceding steps.

Horizontal crab dispersion is directly matched by the crab cavities. However, matching the vertical crab dispersion requires additional knobs to introduce the coupling between the vertical and longitudinal plane. One way is to use the skew quadrupoles positioned between crab cavities, and the other way is to install additional vertical crab cavities. This technical note focuses on correction with vertical crab cavities, proposing a formalism to compute the necessary vertical voltage for these cavities. Through the derived equations, we will identify most effective knobs that can reduce the vertical crab cavity voltage, simplifying the implementation of the crabbing correction scheme. The theoretical formulation delivers crucial insights that will guide the lattice design.

II. MODEL

Several factors contribute to vertical crabbing at the IP, which requires correction. One significant source is the detector solenoid in the EIC, which has a length of 4 m and an integrated strength of up to 12 T · m. For a 275 GeV proton beam, this solenoid introduces a rotation of 6.5 mrad around the longitudinal axis.

Another factor is the proposed tilt of the ESR. In the EIC design, the ESR plane is planned to be rotated by about 200 µrad around the axis that connects from IP6 to IP8 to minimize interference between different storage rings while preserving polarization. As calculated in [5], the dynamic effect of a 200 µrad tilt in the ESR is equivalent to a −4 mrad rotation around the longitudinal axis before the IP, and another 4 mrad rotation after the IP. Unlike the effect from the detector solenoid, the impact of the geometry tilting does not scale with particle energy.

Figure 1 illustrates the local crabbing scheme within the HSR. In this diagram, the yellow blocks labeled "CCB" and "CCA" represent the crab cavities positioned before and after the Interaction Point (IP), respectively. Throughout this note, curly letters denote the linear 6-by-6 transfer matrices. In Fig. 1, $\mathcal{M}_{b,a,r}$ represent the transfer maps from CCB to IP, from IP to CCA, and from CCA back to CCB, respectively. The symbols $\phi_{b,a}$ indicate the rotations around the longitudinal axis before and after the IP, which may result from the ESR tilt, the detector solenoid, or a combination of both. Table I presents the numerical calculation results of $\phi_{b,a}$ at various energies.

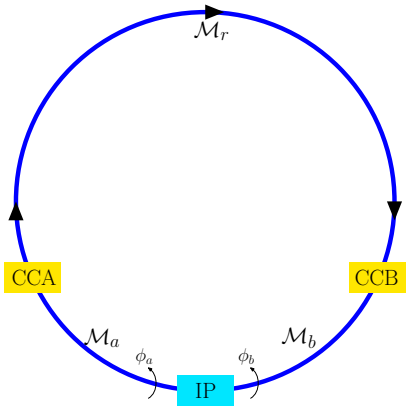


FIG. 1: Schematic of crab crossing scheme.

TABLE I: Rotation angle at different energies.

Energy GeV	Rotation -	Tilting ESR mrad	Detector Solenoid mrad	Both mrad
275	ϕ_b	−4.0	3.3	−0.7
	ϕ_a	4.0	3.3	7.3
100	ϕ_b	−4.0	9.0	5.0
	ϕ_a	4.0	9.0	13.0
41	ϕ_b	−4.0	21.9	17.9
	ϕ_a	4.0	21.9	25.9

III. FORMULA

Without considering longitudinal oscillations, the crab dispersion generated by the thin crab cavity (either CCB or CCA in Fig. 1) is expressed as:

$$\boldsymbol{\zeta}_{b(a)} = \left[0, \frac{\lambda_{b(a),x}}{\sqrt{\beta_{b(a),x}\beta^*_x}}, 0, \frac{\lambda_{b(a),y}}{\sqrt{\beta_{b(a),y}\beta^*_y}}\right]^{\mathrm{T}} \tag{3}$$

where $\beta^*_{x,y}$ are β functions at the IP, and $\lambda_{b(a),x(y)}/\sqrt{\beta_{b(a),x(y)}\beta^*_{x(y)}}$ denoting the horizontal and vertical kick strength. The lattice related parameters $\sqrt{\beta_{b(a),x(y)}\beta^*_{x(y)}}$ are used to normalize the crab cavity strength for simplicity.

Let $M_{b,a,r}$ be the 4-by-4 blocks of linear transfer matrices $\mathcal{M}_{b,a,r}$ depicted in Fig. 1. M_b and M_a can be expressed in terms of Twiss functions as follows:

$$M_b = \begin{bmatrix} \sqrt{\frac{\beta^*_x}{\beta_{b,x}}}\left(\cos\psi_{b,x} + \alpha_{b,x}\sin\psi_{b,x}\right) & \sqrt{\beta_{b,x}\beta^*_x}\sin\psi_{b,x} & 0 & 0 \\ \frac{-\sin\psi_{b,x}+\alpha_{b,x}\cos\psi_{b,x}}{\sqrt{\beta_{b,x}\beta^*_x}} & \sqrt{\frac{\beta_{b,x}}{\beta^*_x}}\cos\psi_{b,x} & 0 & 0 \\ 0 & 0 & \sqrt{\frac{\beta^*_y}{\beta_{b,y}}}\left(\cos\psi_{b,y} + \alpha_{b,y}\sin\psi_{b,y}\right) & \sqrt{\beta_{b,y}\beta^*_y}\sin\psi_{b,y} \\ 0 & 0 & \frac{-\sin\psi_{b,y}+\alpha_{b,y}\cos\psi_{b,y}}{\sqrt{\beta_{b,y}\beta^*_y}} & \sqrt{\frac{\beta_{b,y}}{\beta^*_y}}\cos\psi_{b,y} \end{bmatrix} \tag{4}$$

$$M_a = \begin{bmatrix} \sqrt{\frac{\beta_{a,x}}{\beta^*_x}}\cos\psi_{a,x} & \sqrt{\beta_{a,x}\beta^*_x}\sin\psi_{a,x} & 0 & 0 \\ \frac{-\sin\psi_{a,x}-\alpha_{a,x}\cos\psi_{a,x}}{\sqrt{\beta_{a,x}\beta^*_x}} & \sqrt{\frac{\beta_{x^*}}{\beta_{a,x}}}\left(\cos\psi_{a,x} - \alpha_{a,x}\sin\psi_{a,x}\right) & 0 & 0 \\ 0 & 0 & \sqrt{\frac{\beta_{a,y}}{\beta^*_y}}\cos\psi_{a,y} & \sqrt{\beta_{a,y}\beta^*_y}\sin\psi_{a,y} \\ 0 & 0 & \frac{-\sin\psi_{a,y}-\alpha_{a,y}\cos\psi_{a,y}}{\sqrt{\beta_{a,y}\beta^*_y}} & \sqrt{\frac{\beta_{y^*}}{\beta_{a,y}}}\left(\cos\psi_{a,y} - \alpha_{a,y}\sin\psi_{a,y}\right) \end{bmatrix} \tag{5}$$

where β, α, ψ represent Twiss functions and phase advance. The subscripts "b/a" denote the configuration before or after IP, and "x/y" indicates horizontal or vertical plane. The conditions of $\alpha^*_{x,y} = 0$ are assumed to simplify the equations.

The rotation around longitudinal axis is characterized by the rotation angle ϕ:

$$R(\phi) = \begin{bmatrix} \cos\phi & 0 & \sin\phi & 0 \\ 0 & \cos\phi & 0 & \sin\phi \\ -\sin\phi & 0 & \cos\phi & 0 \\ 0 & -\sin\phi & 0 & \cos\phi \end{bmatrix} \tag{6}$$

The one-turn map M_t at the IP are modeled by the $\beta^*_{x,y}$ and the one-turn phase advance $\mu_{x,y} = 2\pi\nu_{x,y}$, where $\nu_{x,y}$ is the design working point. We assume the betatron coupling introduced by $R(\phi_{b,a})$ has been corrected in M_r.

$$M_t = R_b M_b M_r M_a R_a = \begin{bmatrix} \cos\mu_x & \beta^*_x\sin\mu_x & 0 & 0 \\ -\frac{\sin\mu_x}{\beta^*_x} & \cos\mu_x & 0 & 0 \\ 0 & 0 & \cos\mu_y & \beta^*_y\sin\mu_y \\ 0 & 0 & -\frac{\sin\mu_y}{\beta^*_y} & \cos\mu_y \end{bmatrix} \tag{7}$$

where $R_{b,a}$ is the abbreviation of $R(\phi_{b,a})$.

Let $\boldsymbol{\zeta}^*$ be the closed orbit crab dispersion at the IP. The combined effects of crab dispersion and momentum dispersion are ignored here. After one turn, the closed orbit crab dispersion turns into $M_t\boldsymbol{\zeta}^*$. The contribution from CCB is $R_b M_b \boldsymbol{\zeta}_b$, and the contribution from CCA is $R_b M_b M_r \boldsymbol{\zeta}_a$. According to the definition of closed orbit crab dispersion, we have:

$$\boldsymbol{\zeta}^* = M_t\boldsymbol{\zeta}^* + R_b M_b \boldsymbol{\zeta}_b + R_b M_b M_r \boldsymbol{\zeta}_a \qquad \Longrightarrow \qquad \boldsymbol{\zeta}^* = (I - M_t)^{-1}\left(R_b M_b \boldsymbol{\zeta_b} + M_t R_a^{-1} M_a^{-1} \boldsymbol{\zeta}_a\right) \tag{8}$$

Combining it with Eq. (2), we will have:

$$F\boldsymbol{\lambda} = \left(-\theta_c \cdot 2\sin\pi\nu_x, 0, 0, 0\right)^{\mathrm{T}} \tag{9}$$

where

$$\boldsymbol{\lambda} = \left(\lambda_{b,x}, \lambda_{a,x}, \lambda_{b,y}, \lambda_{a,y}\right)^{\mathrm{T}} \tag{10}$$

and

$$F = \begin{bmatrix} \cos\left(\pi\nu_x - \psi_{b,x}\right) c_b & \cos\left(\pi\nu_x - \psi_{a,x}\right) c_a & \left(\frac{\beta_x^*}{\beta_y^*} c_x c_{b,y} + s_x s_{b,y}\right) s_b & -\left(\frac{\beta_x^*}{\beta_y^*} c_x c_{a,y} + s_x s_{a,y}\right) s_a \\ \sin\left(\pi\nu_x - \psi_{b,x}\right) c_b & -\sin\left(\pi\nu_x - \psi_{a,x}\right) c_a & \left(\frac{\beta_x^*}{\beta_y^*} s_x c_{b,y} - c_x s_{b,y}\right) s_b & \left(\frac{\beta_x^*}{\beta_y^*} s_x c_{a,y} - c_x s_{a,y}\right) s_a \\ -\left(\frac{\beta_y^*}{\beta_x^*} c_y c_{b,x} + s_y s_{b,x}\right) s_b & \left(\frac{\beta_y^*}{\beta_x^*} c_y c_{a,x} + s_y s_{a,x}\right) s_a & \cos\left(\pi\nu_y - \psi_{b,y}\right) c_b & \cos\left(\pi\nu_y - \psi_{a,y}\right) c_a \\ \left(c_y s_{b,x} - \frac{\beta_y^*}{\beta_x^*} s_y c_{b,x}\right) s_b & \left(c_y s_{a,x} - \frac{\beta_y^*}{\beta_x^*} s_y c_{a,x}\right) s_a & \sin\left(\pi\nu_y - \psi_{b,y}\right) c_b & -\sin\left(\pi\nu_y - \psi_{a,y}\right) c_a \end{bmatrix} \tag{11}$$

In the notation used here, c and s represent cos and sin respectively. The subscript $x(y)$, $b(a)$ and $b(a), x(y)$ indicate taking the trigonometric value of $\pi\nu_{x(y)}$, $\phi_{b(a)}$ and $\psi_{b(a),x(y)}$ respectively.

Writing down the exact solution for $\boldsymbol{\lambda}$ can be quite tedious. To streamline our discussion, we can employ a first-order approximation, which is reasonable given the small rotation angles $\phi_{b(a)}$ listed in Table I. This approximation allows us to simplify the calculations without significant loss of accuracy.

Expressing F and $\boldsymbol{\lambda}$ to first order of $\phi_{b(a)}$:

$$\begin{aligned} F &\approx F_{00} + F_{10}\phi_b + F_{01}\phi_a \\ \boldsymbol{\lambda} &\approx \boldsymbol{\lambda}_{00} + \boldsymbol{\lambda}_{10}\phi_b + \boldsymbol{\lambda}_{01}\phi_a \end{aligned} \tag{12}$$

where

$$\begin{aligned} F_{00} &= \begin{bmatrix} \cos\left(\pi\nu_x - \psi_{b,x}\right) & \cos\left(\pi\nu_x - \psi_{a,x}\right) & 0 & 0 \\ \sin\left(\pi\nu_x - \psi_{b,x}\right) & -\sin\left(\pi\nu_x - \psi_{a,x}\right) & 0 & 0 \\ 0 & 0 & \cos\left(\pi\nu_y - \psi_{b,y}\right) & \cos\left(\pi\nu_y - \psi_{a,y}\right) \\ 0 & 0 & \sin\left(\pi\nu_y - \psi_{b,y}\right) & -\sin\left(\pi\nu_y - \psi_{a,y}\right) \end{bmatrix} \\ F_{10} &= \begin{bmatrix} 0 & 0 & \left(\frac{\beta_x^*}{\beta_y^*} s_x c_{b,y} - c_x s_{b,y}\right) & 0 \\ 0 & 0 & \left(\frac{\beta_x^*}{\beta_y^*} s_x c_{b,y} - c_x s_{b,y}\right) & 0 \\ -\left(\frac{\beta_y^*}{\beta_x^*} c_y c_{b,x} + s_y s_{b,x}\right) & 0 & 0 & 0 \\ \left(c_y s_{b,x} - \frac{\beta_y^*}{\beta_x^*} s_y c_{b,x}\right) & 0 & 0 & 0 \end{bmatrix} \\ F_{01} &= \begin{bmatrix} 0 & 0 & 0 & -\left(\frac{\beta_x^*}{\beta_y^*} c_x c_{a,y} + s_x s_{a,y}\right) \\ 0 & 0 & 0 & \left(\frac{\beta_x^*}{\beta_y^*} s_x c_{a,y} - c_x s_{a,y}\right) \\ 0 & \left(\frac{\beta_y^*}{\beta_x^*} c_y c_{a,x} + s_y s_{a,x}\right) & 0 & 0 \\ 0 & \left(c_y s_{a,x} - \frac{\beta_y^*}{\beta_x^*} s_y c_{a,x}\right) & 0 & 0 \end{bmatrix} \end{aligned} \tag{13}$$

Substituting Eq. (12) into Eq. (9), we have:

$$F_{00}\boldsymbol{\lambda}_{00} + \left(F_{00}\boldsymbol{\lambda}_{10} + F_{10}\boldsymbol{\lambda}_{00}\right)\phi_b + \left(F_{00}\boldsymbol{\lambda}_{01} + F_{01}\boldsymbol{\lambda}_{00}\right)\phi_a \approx \left(-\theta_c \cdot 2\sin\pi\nu_x, 0, 0, 0\right)^{\mathrm{T}} \tag{14}$$

From this equation, we can get:

$$\boldsymbol{\lambda}_{00} = F_{00}^{-1} \cdot \left(-\theta_c \cdot 2\sin\pi\nu_x, 0, 0, 0\right)^{\mathrm{T}}, \qquad \boldsymbol{\lambda}_{10} = -F_{00}^{-1}F_{10}\boldsymbol{\lambda}_{00}, \qquad \boldsymbol{\lambda}_{01} = -F_{00}^{-1}F_{01}\boldsymbol{\lambda}_{00} \tag{15}$$

Substituting Eq. (13) into Eq. (15):

$$\begin{aligned}
\lambda_{b,x} &= -\frac{2\theta_c \sin\pi\nu_x \sin\left(\pi\nu_x - \psi_{a,x}\right)}{\sin\left(2\pi\nu_x - \psi_{b,x} - \psi_{a,x}\right)}, \qquad \lambda_{a,x} = -\frac{2\theta_c \sin\pi\nu_x \sin\left(\pi\nu_x - \psi_{b,x}\right)}{\sin\left(2\pi\nu_x - \psi_{b,x} - \psi_{a,x}\right)}, \\
\lambda_{b,y} &= \left[\frac{\left(\frac{\beta_y^*}{\beta_x^*}\right)\cos\psi_{b,x}\sin\left(2\pi\nu_y - \psi_{a,y}\right) - \sin\psi_{b,x}\cos\left(2\pi\nu_y - \psi_{a,y}\right)}{\sin\left(2\pi\nu_y - \psi_{b,y} - \psi_{a,y}\right)}\right]\lambda_{b,x}\phi_b \\
&\quad + \left[\frac{\frac{\beta_y^*}{\beta_x^*}\cos\psi_{a,x}\sin\psi_{a,y} - \sin\psi_{a,x}\cos\psi_{a,y}}{\sin\left(2\pi\nu_y - \psi_{b,y} - \psi_{a,y}\right)}\right]\lambda_{a,x}\phi_a \\
\lambda_{a,y} &= \left[\frac{-\left(\frac{\beta_y^*}{\beta_x^*}\right)\cos\psi_{b,x}\sin\psi_{b,y} + \sin\psi_{b,x}\cos\psi_{b,y}}{\sin\left(2\pi\nu_y - \psi_{b,y} - \psi_{a,y}\right)}\right]\lambda_{b,x}\phi_b \\
&\quad + \left[\frac{-\left(\frac{\beta_y^*}{\beta_x^*}\right)\cos\psi_{a,x}\sin\left(2\pi\nu_y - \psi_{b,y}\right) + \sin\psi_{a,x}\cos\left(2\pi\nu_y - \psi_{b,y}\right)}{\sin\left(2\pi\nu_y - \psi_{b,y} - \psi_{a,y}\right)}\right]\lambda_{a,x}\phi_a
\end{aligned} \tag{16}$$

Noticing that $\psi_{b,x} \approx \psi_{a,x} \approx \pi/2$ and $\beta_y^*/\beta_x^* = 0.09$, the terms labeled by red color in above equations are negligible.

Therefore, $\lambda_{b,y}$ and $\lambda_{a,y}$ can be further simplified as:

$$\begin{aligned}
\lambda_{b,y} &\approx \frac{-\sin\psi_{b,x}\cos\left(2\pi\nu_y - \psi_{a,y}\right)\lambda_{b,x}\phi_b - \sin\psi_{a,x}\cos\psi_{a,y}\lambda_{a,x}\phi_a}{\sin\left(2\pi\nu_y - \psi_{b,y} - \psi_{a,y}\right)} \\
\lambda_{a,y} &\approx \frac{\sin\psi_{b,x}\cos\psi_{b,y}\lambda_{b,x}\phi_b + \sin\psi_{a,x}\cos\left(2\pi\nu_y - \psi_{b,y}\right)\lambda_{a,x}\phi_a}{\sin\left(2\pi\nu_y - \psi_{b,y} - \psi_{a,y}\right)}
\end{aligned} \tag{17}$$

From the above equations, we can draw some conclusions that:

- For a well optimized lattice, $\psi_{b,x} \approx \psi_{a,x} \approx \pi/2$ and $\lambda_{b,x} \approx \lambda_{a,x} \approx -\theta_c$. Given a specific ϕ_b and ϕ_a, it is possible to choose $\psi_{b,y}$ and $\psi_{a,y}$ so that the vertical crabbing is not needed:

$$-\phi_b\cos\left(2\pi\nu_y - \psi_{a,y}\right) + \phi_a\cos\psi_{a,y} = 0, \qquad \text{and} \qquad \phi_b\cos\psi_{b,y} + \phi_a\cos\left(2\pi\nu_y - \psi_{b,y}\right) = 0 \tag{18}$$

- The above constraints may be too strong for practical matching. An alternative approach is to maximize $|\sin(2\pi\nu_y - \psi_{b,y} - \psi_{a,y})|$ in order to minimize the required $\lambda_{b,y}$ and $\lambda_{a,y}$. For instance, with $\nu_y = 0.210, \psi_{b,y} = 126°, \psi_{a,y} = 106°$, we calculate $\sin(2\pi\nu_y - \psi_{b,y} - \psi_{a,y}) = -0.4$. By optimizing $\psi_{b,y}$ and $\psi_{a,y}$ to satisfy $2\pi\nu_y + \psi_{b,y} + \psi_{a,y} = \pm\pi/2 \bmod 2\pi$, the required vertical crabbing could potentially be reduced by a factor of 2.5.

- In practical lattice designs, the range of adjustments available for $\psi_{b,y}$ and $\psi_{a,y}$ may be limited. Therefore, it is advisable to focus directly on minimizing $\lambda_{b,y}$ and $\lambda_{a,y}$ in Eq. (17).

Table II presents a comparison between the required vertical crabbing values calculated from Eq. (9) and Eq. (17). The results clearly demonstrate that Eq. (17) serves as an effective approximation and can be used as a foundation for further optimization efforts.

The comparison of the last five rows in Table IIb, reveals that while the total rotation angle $\phi_b + \phi_a$ remains same across these cases, the required $\lambda_{b,y}$ and $\lambda_{a,y}$ differ significantly. This observation highlights the critical need to finely adjust the Twiss functions, particularly $\psi_{b,y}$ and $\psi_{a,y}$. Without these adjustments, the voltage required for vertical crab cavities or the strength of skew quadrupoles might become excessively high to effectively provide the necessary vertical crabbing.

The optimal values for $\psi_{b,y}$ and $\psi_{a,y}$ vary depending on the specific values of ϕ_b and ϕ_a. Unfortunately, Eq. (17) indicates that there is no universal setting for $\psi_{b,y}$ and $\psi_{a,y}$ that is effective for all combinations of ϕ_b and ϕ_a.

IV. DISCUSSION

The most straightforward method to achieve vertical crabbing is to install additional vertical crab cavities. However, incorporating extra vertical crab cavities involves not only additional costs — such as those for design, fabrication, and installation — but also introduces extra impedance. The impact of this additional impedance on beam dynamics

TABLE II: An numerical example.

(a) Twiss functions when there are no rotations and crab cavities are off

$\psi_{b,x}$ 87°	$\psi_{a,x}$ 88°	β_x^* 80 cm	$\beta_{b,x}$ 1300 m	$\beta_{a,x}$ 1300 m
$\psi_{b,y}$ 126°	$\psi_{a,y}$ 106°	β_y^* 7.2 cm	$\beta_{b,y}$ 30 m	$\beta_{a,y}$ 30 m

(b) Required vertical crabbing: the exact solution is numerically calculated from Eq. (9) and the approximation is calculated from Eq. (17).

ϕ_b	ϕ_a	Exact solution				Approximation			
		$\lambda_{b,x}$	$\lambda_{a,x}$	$\lambda_{b,y}$	$\lambda_{a,y}$	$\lambda_{b,x}$	$\lambda_{a,x}$	$\lambda_{b,y}$	$\lambda_{a,y}$
[mrad]	[mrad]	$\frac{\theta_c}{\sqrt{\beta_{b,x}\beta_x^*}}$	$\frac{\theta_c}{\sqrt{\beta_{a,x}\beta_x^*}}$	$\frac{\theta_c}{\sqrt{\beta_{b,y}\beta_y^*}}$	$\frac{\theta_c}{\sqrt{\beta_{a,y}\beta_y^*}}$	$\frac{\theta_c}{\sqrt{\beta_{b,x}\beta_x^*}}$	$\frac{\theta_c}{\sqrt{\beta_{a,x}\beta_x^*}}$	$\frac{\theta_c}{\sqrt{\beta_{b,y}\beta_y^*}}$	$\frac{\theta_c}{\sqrt{\beta_{a,y}\beta_y^*}}$
−4.0	4.0	0.9612	0.9455	-1.0925×10^{-2}	-1.1714×10^{-2}	0.9610	0.9452	-1.0872×10^{-2}	-1.1652×10^{-2}
3.3	3.3	0.9610	0.9453	4.6720×10^{-3}	-3.0270×10^{-4}	0.9610	0.9452	4.6768×10^{-3}	-3.1351×10^{-4}
−0.7	7.3	0.9613	0.9452	-6.2514×10^{-3}	-1.2014×10^{-2}	0.9610	0.9452	-6.1950×10^{-3}	-1.1966×10^{-2}
0.7	−7.3	0.9613	0.9452	6.2514×10^{-3}	1.2014×10^{-2}	0.9610	0.9452	6.1950×10^{-3}	1.1966×10^{-2}
7.3	−0.3	0.9610	0.9459	1.5333×10^{-2}	1.0806×10^{-2}	0.9610	0.9452	1.5288×10^{-2}	1.0737×10^{-2}
−7.3	0.3	0.9610	0.9459	-1.5333×10^{-2}	-1.0806×10^{-2}	0.9610	0.9452	-1.5288×10^{-2}	-1.0737×10^{-2}

must be thoroughly evaluated. Consequently, the use of additional crab cavities often proves to be infeasible due to these complexities and financial implications.

Another option for providing vertical crabbing is to slightly rotate the crab cavities. In the baseline design of the EIC, each side of the IP is equipped with two cryomodules of 197 MHz and one cryomodule of 394 MHz crab cavities. By rotating each cryomodule to different angles, vertical crabbing can be achieved through various combinations of crab cavity voltages. If crabbing is locally closed, the horizontal and vertical crabbing components can be represented as:

$$\zeta_1^* \propto V_1\cos\theta_1 + V_2\cos\theta_2, \qquad \zeta_3^* \propto V_1\sin\theta_1 + V_2\sin\theta_2$$

where $\theta_{1,2}$ are the rotation angles, and $V_{1,2}$ are the voltages of the crab cavities from the two cryomodules. This method has been discussed at the EIC coupling compensation meeting. It faced significant opposition from crab cavity design experts. The primary concern is the substantial engineering challenges involved in rotating a superconducting cavity.

The remaining viable option is to employ skew quadrupoles, as implemented in the ESR. However, skew quadrupoles also introduce betatron coupling, which complicates the process as betatron coupling correction and crabbing dispersion correction become intertwined. Consequently, it is crucial to develop a strategy that effectively separates these corrections.

Skew quadrupoles can be categorized into two distinct groups according to their specific usage. The first group, positioned between the IP and the upstream or downstream crab cavities, is dedicated to providing vertical crabbing, as shown by the red arrows in Fig. 2. The second group, situated away from the crab cavities, is tasked with addressing betatron coupling , as shown by the blue arrows in Fig. 2.

The correction procedure could be:

(1) **Tuning normal quadrupoles**: Based on the rotation angles ϕ_b and ϕ_a, adjust $\psi_{b,y}$ and $\psi_{a,y}$ to minimize $\lambda_{b,y}$ and $\lambda_{a,y}$ in accordance with Eq. (17).

(2) **Betatron coupling correction**: Turn off the crab cavities but turn on the solenoid, and then adjust the skew quadrupoles, as shown by blue arrows in Fig. 2, to achieve the betatron decoupling.

(3) **Vertical crabbing correction**: Remain the crab cavities off but turn on the skew quadrupoles between crab cavities, as shown by red arrows in Fig. 2. These skew quadrupole strength are calculated from Eq. (17). Sub-

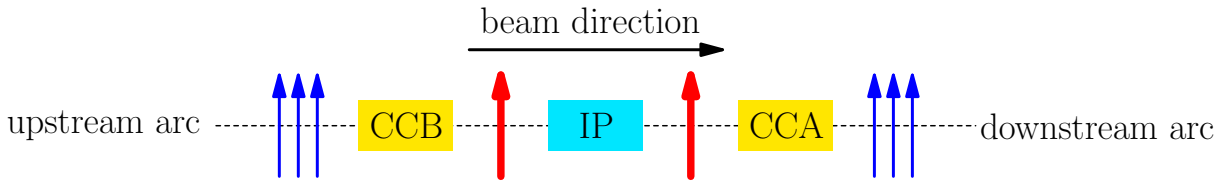


FIG. 2: Schematic of the correction scheme using skew quadrupoles for vertical crabbing and betatron coupling. The red arrows indicate skew quadrupoles dedicated to vertical crabbing, while the blue arrows represent those used for betatron coupling correction.

sequently, readjust the skew quadrupoles outside crab cavities (blue arrows in Fig. 2) once more to fine-tune the betatron decoupling.

(4) **Fine-tuning the result**: Turn on the crab cavities, and adjust all skew quadrupoles to exactly match the conditions in Eq. (2)

V. SUMMARY

In this technical note, we have examined the challenges and solutions associated with vertical crabbing in the EIC-HSR. We discussed the necessity of precise matching of crab and momentum dispersion to achieve optimal beam-beam performance and presented a general procedure for correcting dispersion and betatron coupling with skew quadrupoles in the HSR. The theoretical formula is derived to minimize the required vertical crabbing. The methodologies and strategies outlined in this note provide a robust framework for addressing vertical crabbing in the HSR, ensuring the EIC can achieve its luminosity goals. Future work will implement this correction scheme in the HSR lattice design.

ACKNOWLEDGMENTS

The author extends gratitude to F. Willeke for the manuscript review and numerous insightful suggestions.

[1] F. Willeke and J. Beebe-Wang, *Electron Ion Collider Conceptual Design Report 2021*, Tech. Rep. (Brookhaven National Lab.(BNL), Upton, NY (United States); Thomas Jefferson National Accelerator Facility (TJNAF), Newport News, VA (United States), 2021).

[2] D. Xu *et al.*, Detector Solenoid Compensation in the EIC Electron Storage Ring, in *Proc. IPAC'22*, International Particle Accelerator Conference No. 13 (JACoW Publishing, Geneva, Switzerland, 2022) pp. 1972–1975.

[3] J. S. Berg, R. B. Palmer, and H. Witte, Lattice design for the interaction region of the electron-ion collider, in *Proc. IPAC'23*, IPAC'23 - 14th International Particle Accelerator Conference No. 14 (JACoW Publishing, Geneva, Switzerland, 2023) pp. 909–912.

[4] D. Xu, Y. Luo, and Y. Hao, Combined effects of crab dispersion and momentum dispersion in colliders with local crab crossing scheme, Phys. Rev. Accel. Beams **25**, 071002 (2022).

[5] D. Xu, Y. Hao, D. Holmes, Y. Luo, C. Montag, J. Qiang, and F. J. Willeke, Beam-Beam Interaction for Tilted Storage Rings, in *Proc. IPAC'22*, International Particle Accelerator Conference No. 13 (JACoW Publishing, Geneva, Switzerland, 2022) pp. 1968–1971.